

Anomalous Nonlinear Optical Selection Rules in Metallic Quantum Wells

Shilong Li, Haoliang Qian, and Zhaowei Liu*

Intersubband transitions (ISBTs) in conduction-band quantum wells (QWs) have attracted tremendous attention for their high technological potential, ranging from quantum cascade lasers, quantum well infrared photodetectors, to various nonlinear optical elements. One of the main characteristics of using the ISBTs is their polarization selection rule, which forbids a normal-incidence geometry. Here, it is shown that the ISBT selection rule is not strict on optical nonlinearities in metallic QWs (MQWs). The nonlinear process of second harmonic generation nearly follows the selection rule, while the optical Kerr nonlinear process severely deviates from it. The anomalous optical selection rules result from the non-negligible ultrafast electron–electron scattering in these plasmonic systems, and a coupled mode theory is provided to get a physical grasp of the problem. The flexible selection rule in MQWs could bring drastic improvements in efficiency and diversity of ISBT-based devices.

1. Introduction

The continuous translational symmetry of semiconductor quantum well (SQW) heterostructures in their growth plane gives rise to a polarization selection rule for their conduction-band intersubband transitions (ISBTs)—only the electric field component along the quantum-well (QW) growth direction can interact with the ISBT. The presence of this selection rule largely degrades the performance of ISBT-based optoelectronic devices.^[1–7] Much effort has thus been directed toward relaxing the selection rule by breaking the continuous translational symmetry of QWs.^[7] Nevertheless, the polarization selection rule imposed on these conduction-band ISBTs is well followed in most common SQWs.^[8]

Dr. S. Li, Dr. H. Qian, Prof. Z. Liu
Department of Electrical and Computer Engineering
University of California, San Diego
9500 Gilman Dr, La Jolla, CA 92093, USA
E-mail: zhaowei@ucsd.edu

Prof. Z. Liu
Materials Science and Engineering
University of California, San Diego
9500 Gilman Dr, La Jolla, CA 92093, USA

Prof. Z. Liu
Center for Memory and Recording Research
University of California, San Diego
9500 Gilman Dr, La Jolla, CA 92093, USA

 The ORCID identification number(s) for the author(s) of this article can be found under <https://doi.org/10.1002/adfm.202000829>.

DOI: 10.1002/adfm.202000829

In a different context, however, less attention has been paid to the ISBT selection rules in metallic QWs (MQWs). In these plasmonic systems, due to the plasma screening effect,^[9] it is the screened field, not the incident field, to which the electrons respond.^[10] As a result, the dielectric function of MQWs is assumed to be scalar,^[10–15] meaning that there are no polarization selection rules applicable to their linear optical properties. It was not until very recently, however, that the optical nonlinearities of MQWs have been experimentally explored, enabled by the success in fabrication of ultrathin continuous metallic films on top of a dielectric substrate.^[13,16,17] Surprisingly, ISBT peaks, the signature of the quantum size effect in QWs, have been observed in the nonlinear coefficient spectra of these MQWs^[16,17]; the

manifestation of the ISBTs is an extraordinary enhancement of these optical nonlinearities which are several orders of magnitude larger than those of traditional nonlinear materials at visible/near-infrared (NIR) frequencies. However, no systematic study of the ISBT selection rules for optical nonlinearities in MQWs has been made. The lack of such a study, on one hand, hinders the extensive applications of the ISBT-enabled extreme optical nonlinearities in the technologically more important visible/NIR spectrum range, and on the other hand, restricts the development of the theory of ISBTs in plasmonic systems.

In this work, we report a systematic study of ISBT selection rules imposed on the 2nd and 3rd order optical nonlinearities of MQWs. The MQWs were made of refractory materials, that is, TiN and Al₂O₃, which could be fabricated in ultrathin films with atomically flat interfaces over a large area,^[18,19] as shown in the right inset of **Figure 1**. Such a high-quality MQW heterostructure is crucial in revealing the quantum size effect of ISBTs, while its refractory property makes possible the ultrahigh-intensity nonlinear optical measurements and applications.

2. Results and Discussion

2.1. ISBTs in SQWs and MQWs

First, we briefly discuss the fundamental differences between SQWs and MQWs with respect to their intrinsic plasma frequencies and typical working frequencies for nonlinear optics (Figure 1). For ISBT in SQWs, the working frequencies are generally much higher than the plasma frequencies (Figure 1),

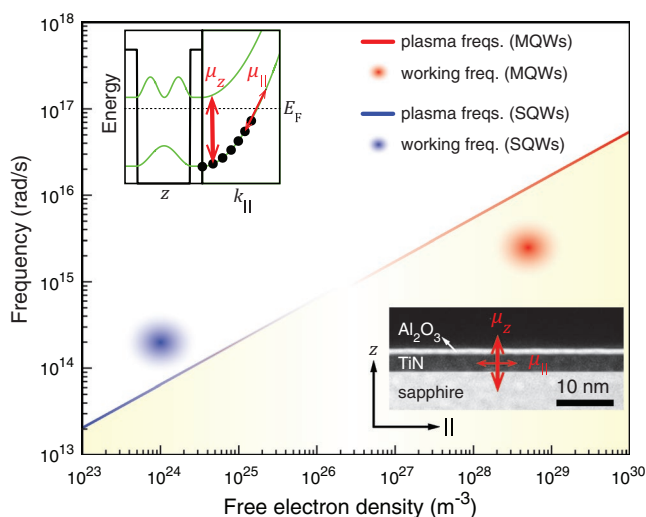


Figure 1. Comparison between SQWs and MQWs. The diagram shows the relative position between the typical working (circular shadows) and intrinsic plasma (solid lines) frequencies. The optical responses in the light-yellow shadowed region would be affected by the plasma screening effect. The GaAs-based SQWs and TiN-based MQWs are used for this comparison. Left inset: schematic of band diagram and the corresponding dispersion of subbands. The red arrows indicate the ISBT and the intrasubband transition, and the corresponding electric dipoles μ_z and μ_{\parallel} are depicted in the right inset. Right inset: transmission electron microscopy (TEM) cross-section of a single layer of TiN MQW. The layer on top of the MQW is a protective layer used only for TEM cross-section preparation during the focused ion beam cutting process.

so that the plasma screening effect is negligible. Since the dipole matrix element μ_z of ISBTs is a few orders of magnitude larger than that of the intrasubband transition μ_{\parallel} (Section S1, Supporting Information), the optical response of SQWs is

dominated by their ISBTs. Therefore, the polarization selection rule of ISBTs is imposed on the optical properties of SQWs. By contrast, the working frequencies of MQWs are usually in the visible/NIR spectral range, and are thus below the plasma frequencies (Figure 1). As a result, the plasma screening effect would mitigate the differences between μ_z and μ_{\parallel} , altering the polarization selection rule, as demonstrated in what follows.

2.2. ISBT Selection Rule on Second Harmonic Generation

Now, we begin with the ISBT selection rule for the 2nd order nonlinear effect, that is, the second harmonic generation (SHG), from MQWs (Figure 2). The MQW sample consists of coupled TiN wells (1.0 and 2.2 nm) separated by an Al_2O_3 barrier (0.5 nm), such that a double ISBT at the wavelength of 920 nm is produced.^[17] Figure 2a shows the SHG measurement apparatus. We have shown^[17] a peak centered at the double transition wavelength in the measured 2nd order susceptibility $\chi^{(2)}$ spectrum from this MQW sample, revealing the origin of ISBT enhancement. The $\chi^{(2)}$ achieved is as high as $\approx 1500 \text{ pm V}^{-1}$, so that the contribution from intrasubband transitions ($\approx 1 \text{ pm V}^{-1}$) can be ignored. A restrictive selection rule would be expected in SHG if there is no coupling between the intrasubband transition and the ISBT: SHG intensity I_{SHG} from ISBTs is proportional to the square of the electric field intensity along the growth direction, that is, $I_{\text{SHG}} \propto I_z^2$, where $I_z \propto E^2 \sin^2(\varphi)$, E is the incident electric field, and φ is the polarization angle, so that $I_{\text{SHG}} \propto \sin^4(\varphi)$. Such a quartic dependence of SHG with respect to $\sin(\varphi)$ in this MQW sample under 0.48 GW cm^{-2} peak intensity illumination was observed.^[17]

The obedience of SHG to the ISBT selection rule in the MQW seems to indicate that the plasma screening effect does

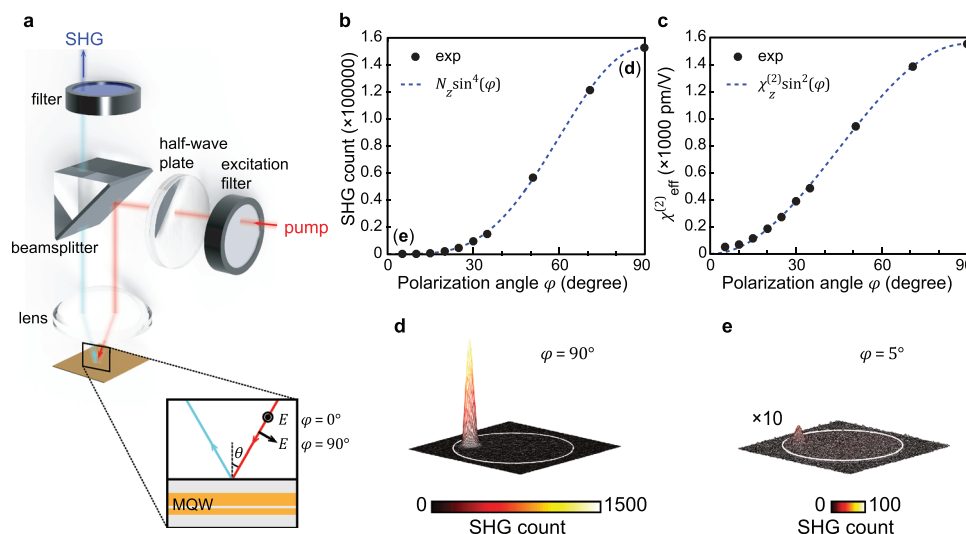


Figure 2. Selection rule for SHG in MQWs. a) Diagram of the SHG measurement setup. The polarization angle φ of the pumping light is varied by a half-wave plate. The incident angle θ is fixed at 45° . The reflected wave is collected by the same lens used for the incident wave, and then passed through a short-pass filter, such that only SHG signals are recorded. b) Polarization dependence of SHG emissions and c) the corresponding $\chi_{\text{eff}}^{(2)}$. N_z is the SHG count at $\varphi = 90^\circ$. d) Charge coupled device images at the back-aperture plane showing the coherence of the SHG signal from p -polarized ($\varphi = 90^\circ$) and e) nearly s -polarized ($\varphi = 5^\circ$) pumping light. 920 nm pulses (100 fs pulse width, 80 MHz repetition rate, $5 \mu\text{m}$ spot) with a peak intensity of 4.8 GW cm^{-2} were used. The white circle indicates the maximum collection angle of the lens. It is worth noting that the background signal throughout the entire back-aperture plane is mainly the result of fluorescence emissions due to two-photon absorption.

not play any role in the SHG nonlinear process. To double-check this rather unusual experimental observation, the SHG selection rule was examined under a relatively high-intensity illumination, that is, 4.8 GW cm^{-2} peak intensity—one order of magnitude higher than the previous value. Figure 2d,e shows the back-aperture images, respectively, for the *p*-polarized ($\varphi = 90^\circ$) and nearly *s*-polarized ($\varphi = 5^\circ$) SHGs, at a fixed incident angle of $\theta = 45^\circ$. It was observed that the nearly *s*-polarized SHG signals were localized at the collection angle in the back-aperture plane, the same as that of the *p*-polarized SHG but with a much smaller amplitude; this is the signature of a coherent (instantaneous) SHG^[17] (Section S2, Supporting Information). The total instantaneous SHG emissions (I_{SHG}) within the collection angle were obtained at various polarization states, and the results are summarized in Figure 2b. The quartic dependence of I_{SHG} on $\sin(\varphi)$ sets an experimental difficulty for directly measuring the instantaneous SHG emission when the polarization angle φ approaches 0° —that is a pure *s*-polarization; instead, the extrapolation method was applied to obtain the pure *s*-polarization SHG emission. As shown in Figure 2b, the SHG closely follows the ISBT selection rule even under this relatively high-intensity illumination. A slight deviation from the selection rule becomes discernable by evaluating the effective $\chi_{\text{eff}}^{(2)}$ that has a quadratic dependence on $\sin(\varphi)$, that is, $\chi_{\text{eff}}^{(2)} = \sqrt{I_{\text{SHG}}/I_z} \chi_z^{(2)} = \chi_z^{(2)} \sin^2(\varphi)$, where I_z and $\chi_z^{(2)}$ are, respectively, the SHG intensity and the corresponding $\chi_{\text{eff}}^{(2)}$, at $\varphi = 90^\circ$. The $\chi_{\text{eff}}^{(2)}$ is shown in Figure 2c and a clearer but still minute deviation from the ISBT selection rule was observed in SHG in MQWs.

2.3. Time Evolution of ISBTs in MQWs

We attribute the slight relaxation of the ISBT selection rule for SHG in MQWs to the coupling-induced ISBT from intrasubband transitions (Figure 3). The incident E_{\parallel} component of the pumping light drives the intrasubband transition of electrons (Figure 3a), but the resultant instantaneous nonlinearity, such as the SHG investigated here, is too weak to be observed in the experiments. Nevertheless, the ultrafast electron–electron scattering due to the plasma screening effect in MQWs has to be taken into account, for it enables conversion of E_{\parallel} to E_z (Figure 3a). So long as this conversion has the possibility to occur within a few tenths of an optical cycle (Figure 3b), that is, no longer than a few 100 as,^[20] SHG due to ISBTs from the converted E_z could be observable. We believe that the deviation of the ISBT selection rule demonstrated in Figure 2 is the result of this electron–electron scattering-induced $E_{\parallel} \rightarrow E_z$ conversion. For the instantaneous SHG process, only the initial small portion of time duration is relevant; thus, the degree of the deviation is limited. On the other hand, we expect to observe a severe selection-rule break on non-instantaneous nonlinearities, such as the optical Kerr nonlinearity (Figure 3b), as demonstrated below.

2.4. ISBT Selection Rule on Optical Kerr Nonlinearity

The ISBT selection rule for optical Kerr nonlinearity from an MQW was also examined and the results are summarized in

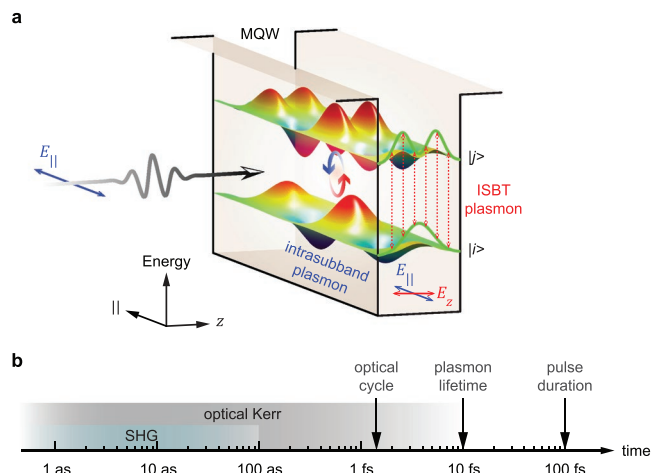


Figure 3. Ultrafast electron dynamics in MQWs. a) Diagram of ISBT induced by coupling between intrasubband plasmons in MQWs. Free electrons in the MQWs undergo a direct intrasubband transition, that is, intrasubband plasmon, under the excitation of a laser pulse with only E_{\parallel} . ISBTs (red dashed lines) could arise as the result of the conversion of E_z from the incident E_{\parallel} caused by ultrafast electron–electron scattering. b) Time scales of various optical nonlinear processes in MQWs. Coherent SHG typically occurs within a few 100 as, while optical Kerr nonlinearity may come from non-instantaneous effects up to a few 10 fs, which is related to the plasmon lifetime.

Figure 4. Z-scan measurements^[21] were implemented on a single layer of 2 nm TiN MQW (Figure 4a). The insets i and ii of Figure 4a show, respectively, the open and closed aperture signals, by which the complex Kerr coefficient n_2 was extracted. The extracted n_2 at the incident angle $\theta = 40^\circ$ is shown in Figure 4b. The n_2 is $(8.9-1.6i) \times 10^{-13} \text{ m}^2 \text{ W}^{-1}$, which is several orders of magnitude higher than that of traditional nonlinear materials,^[20] and is the direct evidence of ISBTs, as has been demonstrated in gold MQWs.^[16] The ISBT selection rule, if not broken, gives the n_2 a $\sin(\theta)$ dependence; for example, the n_2 at $\theta = 10^\circ$ is expected to be 27% of that at $\theta = 40^\circ$. However, from the measured wavelength dependence of n_2 at $\theta = 10^\circ$ (Figure 4c), we observe that it is about 50% of the amplitude of that at $\theta = 40^\circ$, indicating a significant break of the ISBT selection rule.

The incident angle dependence of the 3rd order susceptibility $\chi_{\text{eff}}^{(3)}$, obtained from n_2 at the wavelength of 930 nm, is shown in Figure 4d, and a big deviation from a $\sin(\theta)$ dependence was observed. As mentioned above, there is an $E_{\parallel} \leftrightarrow E_z$ conversion due to ultrafast electron–electron scattering in MQWs, which is responsible for the ISBT selection-rule relaxation: the longer the timescale that a nonlinear process takes, the larger is the degree of selection-rule violation. The optical Kerr process lasts as long as the plasmon dissipates, which takes about one order of magnitude longer than the optical cycle.^[22] Therefore, the ISBT selection rule is severely broken for the Kerr nonlinearity, as expected in Figure 3. The pulse width used in the z-scan measurements (100 fs) is much longer than the plasmon lifetime,^[22] so that it plays only a minor role in the selection-rule break; for example, a very similar angle dependence of $\chi_{\text{eff}}^{(3)}$ was observed when 125 fs pulses were used (Figure S2 and Section S3, Supporting Information).

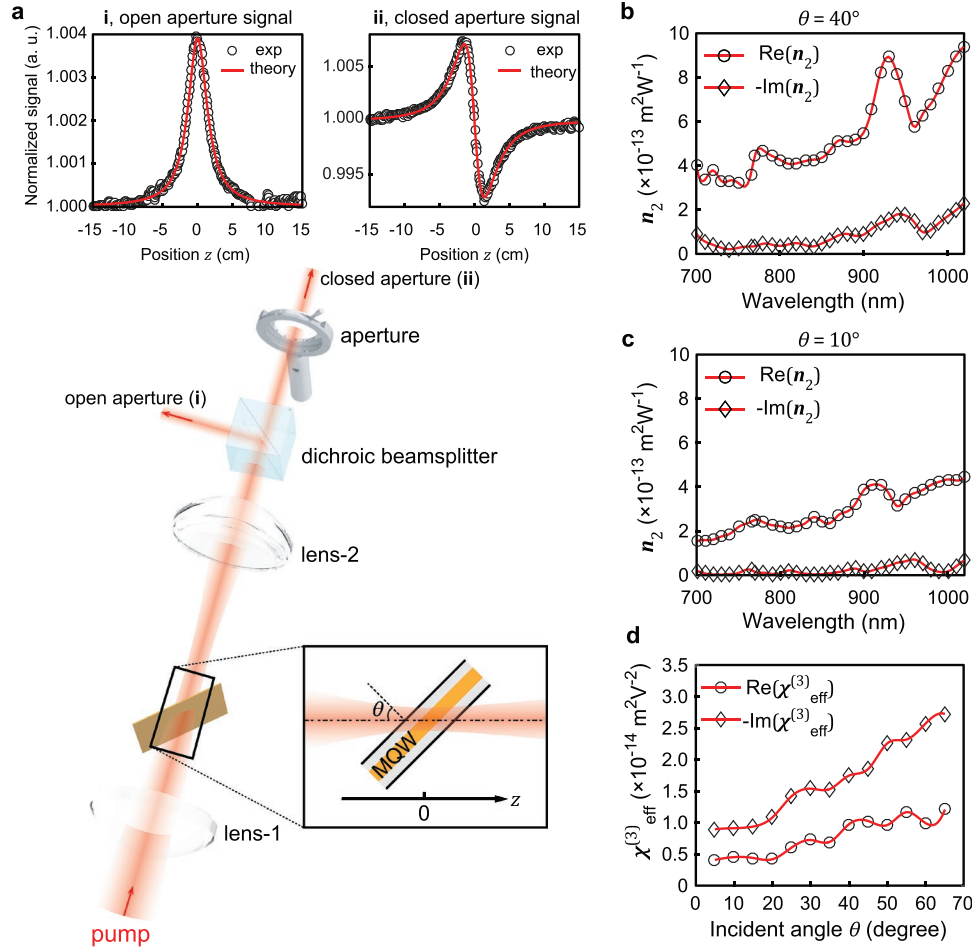


Figure 4. Selection rule for optical Kerr nonlinearity in MQWs. a) Diagram of z-scan experiments. Pumping pulses (100 fs pulse width, 80 MHz repetition rate, 90 μm beam radius) are focused using a lens (lens-1) onto an MQW sample with incident angle θ , while the sample is moved along the optical axis near the focus of the lens. Insets i and ii show, respectively, the measured open and closed aperture z-scan curves with the wavelength of 930 nm at $\theta = 40^\circ$. The imaginary part of n_2 is obtained from the open aperture curve, while the closed aperture curve is used to determine its real part. Wavelength dependence of the extracted n_2 at b) $\theta = 40^\circ$ and c) $\theta = 10^\circ$. d) Incident angle dependence of $\chi_{\text{eff}}^{(3)}$ at the wavelength of 930 nm.

2.5. Coupled Mode Theory

In our intuitive understanding of this selection-rule break, the coupling between the intrasubband-transition modes and the continuum of degrees of freedoms of the surrounding many-body environment is an essential element to describe the $E_{\parallel} \leftrightarrow E_z$ conversion. Therefore, the coupled mode theory (CMT)^[23] was applied (Figure 5a). The equations for the time-varying amplitudes of two intrasubband transition modes (nonzero $a_{\parallel,i}$ and $a_{\parallel,j}$) and the resultant ISBT mode ($a_{z,ij}$) can be written as follows

$$\frac{da_{\parallel,i}}{dt} = (i\omega_{\parallel,i} - \Gamma_{\parallel,i})a_{\parallel,i} + iK_{\parallel,ij}a_{\parallel,j} + i\eta_{c,iz}a_{z,ij} + (\langle K_{\parallel,i} |^* | s^+ \rangle) \cos(\theta) \quad (1a)$$

$$\frac{da_{\parallel,j}}{dt} = (i\omega_{\parallel,j} - \Gamma_{\parallel,j})a_{\parallel,j} + iK_{\parallel,ij}a_{\parallel,i} + i\eta_{c,jz}a_{z,ij} + (\langle K_{\parallel,j} |^* | s^+ \rangle) \cos(\theta) \quad (1b)$$

$$\frac{da_{z,ij}}{dt} = (i\omega_{z,ij} - \Gamma_{z,ij})a_{z,ij} + i\eta_{c,iz}a_{\parallel,i} + i\eta_{c,jz}a_{\parallel,j} + (\langle K_z |^* | s^+ \rangle) \sin(\theta) \quad (1c)$$

$$|s^-\rangle = \mathbb{C} |s^+\rangle + a_{\parallel,i} |D_{\parallel,i}\rangle + a_{\parallel,j} |D_{\parallel,j}\rangle + a_{z,ij} |D_z\rangle \quad (1d)$$

where $|s^\pm\rangle = (s_1^\pm, s_2^\pm)$ represents the amplitudes of the input/output scattering channels, such that $|s|^2$ and $|a|^2$ are, respectively, the energy flux per unit time going through the system and the total energy stored in the plasmon mode. $|K\rangle$ and $|D\rangle$ are coupling coefficients between the scattering channels and the plasmons, while the direct scattering amplitude is given by the scattering matrix \mathbb{C} ; energy conservation and time-reversal symmetry^[23] require these coefficients to be related by $|K\rangle = |D\rangle$ and $\langle D |^* \mathbb{C} = -|D\rangle$. The two intrasubband plasmons with frequencies $\omega_{\parallel,i}$ and $\omega_{\parallel,j}$ directly exchange energy because of the overlap of their wavefunctions described by the coupling constant $K_{\parallel,ij}$ ^[24]; they also decay to the same continuum with the decay rates $\Gamma_{\parallel,i}$ and $\Gamma_{\parallel,j}$ and thus couple to each other in the continuum, not only within the growth plane but also along the z direction, which gives rise to an ISBT at rates $\eta_{c,iz}$ and $\eta_{c,jz}$. This through-continuum coupling-induced ISBT quantifies the

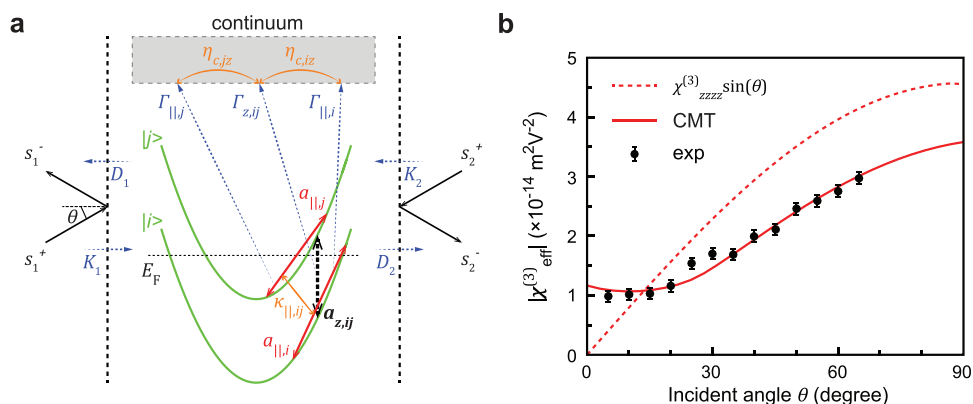


Figure 5. CMT model of ISBT selection-rule break in MQWs. a) Proposed mechanism of ISBT induced by coupling between intrasubband transitions through an energy continuum. The vertical dashed lines indicate the reference planes for input/output waves, while the top grey rectangle represents the continuum to which the intrasubband plasmons decay and are coupled, such that a selection-rule—forbidden ISBT is enabled. b) CMT fitting of optical Kerr selection-rule experiments. The standard deviation of the experimental data is indicated by the error bars. The solid red curve presents the CMT fitting of the experimental results, while the corresponding ISBT selection-rule prediction is given by the dashed red line.

$E_{\parallel} \leftrightarrow E_z$ conversion process responsible for the ISBT selection-rule break in MQWs.

The procedure of CMT fitting of selection-rule experiments is described in Section S4, Supporting Information. For optical Kerr nonlinearity, the $E_{\parallel} \leftrightarrow E_z$ conversion rates $\eta_{c,iz}$ and $\eta_{c,jz}$ are the only unknown parameters and are thus used for the fitting. Since the plasmon frequency of the j th subband is below the driving frequency ω_0 (wavelength 930 nm), we set $\eta_{c,jz} = 0$. Figure 5b shows the CMT fitting of the optical Kerr nonlinearity by means of the least square method and $\eta_{c,iz} = 0.77\omega_0$ was obtained. Along the same line of reasoning, the SHG selection-rule experiments were also fitted by the CMT model, which determines a time duration of 115 as for an SHG process, as expected from Figure 3—that is no longer than a few 100 as.^[20] Therefore, it is clear how the timescale that a nonlinear process takes in MQWs determines the degree of the ISBT selection-rule break: for instantaneous nonlinearities such as SHG (Figure 2), only the first few 100 as is relevant so that the break is very small, while it is severe for the non-instantaneous Kerr nonlinearity (Figure 4) taking place within the entire plasmon lifetime (a few 10 fs).

3. Conclusion

In conclusion, we have demonstrated giant optical nonlinearities at the visible/NIR frequencies from TiN-based MQWs and presented a systematic investigation on the nonlinear selection rule, which shows that the ISBT selection rule for these giant optical nonlinearities in MQWs can be broken, and the degree of the break is strongly related to the timescale that the nonlinear process takes. The relaxation of this fundamental barrier is attributed to the ultrafast electron–electron interactions in these plasmonic systems, and a CMT is provided not only to show a clear physical picture of the problem, but also to quantify relative parameters for further applications. The ISBT induced by the electron–electron interactions between intrasubband plasmons opens the possibility of new coherent manipulation of optical nonlinearities by adjusting the electron density. Finally, the giant optical nonlinearities without a strict selection

rule in MQWs made of refractory materials can be used for designing high-performance ISBT-based devices covering the visible to infrared spectra, providing new degrees of freedom for the optimal design of an optical nonlinear system.

Supporting Information

Supporting Information is available from the Wiley Online Library or from the author.

Acknowledgements

The authors acknowledge financial support from National Science Foundation—Division of Materials Research (Grant No. 1610538) and DARPA DSO-NLM Program (Grant No. HR00111820038). S.L. acknowledges the financial support of the International Postdoctoral Exchange Fellowship Program (No. 20170010).

Conflict of Interest

The authors declare no conflict of interest.

Author Contributions

S.L. and H.Q. contributed equally to this work. S.L., H.Q., and Z.L. conceived the idea. S.L. and H.Q. performed the theoretical calculation and numerical simulation. H.Q. performed the sample growth and performed the experiments. S.L., H.Q., and Z.L. wrote the manuscript. All authors analyzed the data and revised the manuscript. Z.L. supervised the research.

Keywords

intersubband transitions, metallic quantum wells, optical nonlinearity, optical selection rule

Received: January 28, 2020
Revised: February 25, 2020
Published online: March 20, 2020

- [1] J. Faist, F. Capasso, D. L. Sivco, C. Sirtori, A. L. Hutchinson, A. Y. Cho, *Science* **1994**, 264, 553.
- [2] M. S. Vitiello, G. Scalari, B. Williams, P. De Natale, *Opt. Express* **2015**, 23, 5167.
- [3] B. F. Levine, *J. Appl. Phys.* **1993**, 74, R1.
- [4] D. Palaferri, Y. Todorov, A. Bigioli, A. Mottaghizadeh, D. Gacemi, A. Calabrese, A. Vasanelli, L. Li, A. G. Davies, E. H. Linfield, F. Kapsalidis, M. Beck, J. Faist, C. Sirtori, *Nature* **2018**, 556, 85.
- [5] E. Rosencher, A. Fiore, B. Vinter, V. Berger, P. Bois, J. Nagle, *Science* **1996**, 271, 168.
- [6] J. Lee, M. Tymchenko, C. Argyropoulos, P.-Y. Chen, F. Lu, F. Demmerle, G. Boehm, M.-C. Amann, A. Alù, M. A. Belkin, *Nature* **2014**, 511, 65.
- [7] H. C. Liu, F. Capasso, *Intersubband Transitions in Quantum Wells: Physics and Device Applications*, 1st ed., Semiconductors and Semimetals vol. 62, Elsevier, New York **1999**.
- [8] H. C. Liu, M. Buchanan, Z. R. Wasilewski, *Appl. Phys. Lett.* **1998**, 72, 1682.
- [9] H. Haug, S. W. Koch, *Quantum Theory of the Optical and Electronic Properties of Semiconductors*, 5th ed., World Scientific Publishing Company, Singapore **2009**.
- [10] D. M. Wood, N. W. Ashcroft, *Phys. Rev. B* **1982**, 25, 6255.
- [11] J. Dryzek, A. Czaplak, *Phys. Rev. Lett.* **1987**, 58, 721.
- [12] M. Cini, P. Ascarelli, *J. Phys. F: Met. Phys.* **1974**, 4, 1998.
- [13] H. Qian, Y. Xiao, D. Lepage, L. Chen, Z. Liu, *Nanophotonics* **2015**, 4, 413.
- [14] R. A. Maniyara, D. Rodrigo, R. Yu, J. Canet-Ferrer, D. S. Ghosh, R. Yongsunthon, D. E. Baker, A. Rezikyan, F. J. García de Abajo, V. Pruneri, *Nat. Photonics* **2019**, 13, 328.
- [15] Y. Silberberg, T. Sands, *IEEE J. Quantum Electron.* **1992**, 28, 1663.
- [16] H. Qian, Y. Xiao, Z. Liu, *Nat. Commun.* **2016**, 7, 13153.
- [17] H. Qian, S. Li, C.-F. Chen, S.-W. Hsu, S. E. Bopp, Q. Ma, A. R. Tao, Z. Liu, *Light: Sci. Appl.* **2019**, 8, 13.
- [18] G. V. Naik, B. Saha, J. Liu, S. M. Saber, E. A. Stach, J. M. K. Irudayaraj, T. D. Sands, V. M. Shalaev, A. Boltasseva, *Proc. Natl. Acad. Sci. U. S. A.* **2014**, 111, 7546.
- [19] P. Patsalas, N. Kalfagiannis, S. Kassavetis, *Materials* **2015**, 8, 3128.
- [20] R. W. Boyd, *Nonlinear Optics*, Academic Press, Orlando, FL **2008**.
- [21] M. Sheik-Bahae, A. A. Said, T. H. Wei, D. J. Hagan, E. W. V. Stryland, *IEEE J. Quantum Electron.* **1990**, 26, 760.
- [22] J. B. Khurgin, *Nat. Nanotechnol.* **2015**, 10, 2.
- [23] S. Fan, W. Suh, J. D. Joannopoulos, *J. Opt. Soc. Am. A* **2003**, 20, 569.
- [24] Y. Todorov, *Phys. Rev. B* **2015**, 91, 125409.